Neutron Energy Spectrum Measurement using CLYC7-based Compact Neutron Emission Spectrometer in the Large Helical Device

S. Sangaroon,[a,b,1] K. Ogawa,[a,c] M. Isobe,[a,c] M.I. Kobayashi,[a,c] Y. Fujiwara,[a] S. Kamio,[a] H. Yamaguchi,[a,c] R. Seki,[a,c] H. Nuga,[a] S. Toyama,[d] M. Miwa,[d] S. Matsuyama,[d] E. Takada,[e] S. Murakami,[f] G.Q. Zhong,[g] and M. Osakabe[a,c]

[a] *National Institute for Fusion Science, National Institutes of Natural Sciences, 322-6 Oroshi-cho, Toki 509-5292, Japan*

[b] *Faculty of Science, Mahasarakham University, Maha Sarakham, 44150, Thailand*

[c] *The Graduate University for Advanced Studies, SOKENDAI, 322-6 Oroshi-cho, Toki 509-5292, Japan*

[d] *Tohoku University, 6-6 Aoba, Aramaki, Aoba-ku, Sendai, 980-8579, Japan*

[e] *National Institute for Technology, Toyama College, Hongo-machi, Toyama city, Toyama, 939-8630, Japan*

[f] *Department of Nuclear Engineering, Kyoto University, Nishikyo, Kyoto, 615-8540, Japan*

[g] *Institute of Plasma Physics, Chinese Academy of Sciences, Hefei 230031, People's Republic of China*

E-mail: siriyaporn.s@msu.ac.th

ABSTRACT: Tangential compact neutron emission spectrometer (CNES) based on the Cs_2LiYCl_6:Ce with ^{7}Li-enrichment (CLYC7) scintillator is newly installed in the Large Helical Device (LHD). Measurement of neutron energy spectrum was performed using CNES in tangential neutral beam (NB) heated deuterium plasma discharges. The Doppler shift of neutron energy according to the direction of tangential NB injection has been obtained. When the fast ions moving away from the CNES, lower shifted neutron energy is obtained, whereas the upper shifted neutron energy is obtained when the fast ions moving toward the CNES. The obtained neutron energy is almost consistent with the virgin deuterium-deuterium neutron energy evaluated by the simple two-body kinematic calculation.

KEYWORDS: Compact neutron emission spectrometer; CLYC7; Doppler effect; LHD; Neutral beam heating.

[1] Corresponding author.

Contents

1. Introduction

Understanding of fast ion confinement plays an important role to make effective plasma heating and to achieve high-performance plasmas in existing fusion devices [1], since the plasmas are mainly heated by the fast ions, generated by neutral beam (NB) injection and/or by ion cyclotron resonant frequency (ICRF) heating. In particular, the impact of fast-ion-driven magnetohydrodynamic (MHD) instability on fast ion transport is one of the attractive topics in fusion reserch [2]. The Large Helical Device (LHD) is characterized by equipping a high-acceleration energy negative-ion-source-based neutral beam (N-NB) injection heating with tangential direction. The study of fast ion transport caused by fast-ion-driven MHD instabilities using the N-NBs has been reported [3]. In the LHD hydrogen plasma experiments, the fast ion transport and loss induced by the toroidicity-induced Alfvén eigenmode have been studied using fast ion diagnostics, e.g., a neutral particle analyzer [4] and fast ion loss detector [5]. Furthermore, comparisons of the experimental results and numerical simulations have been intensively conducted [6, 7]. Since March 2017, plasma experiments using deuterium gas have been performed in the LHD. The study of fast ion confinement has been well advanced using comprehensive neutron diagnostics [8-11], since neutrons are mainly created by fusion reactions between thermal ions and fast ions generated by NBs [12]. The fast ion transport and loss due to the energetic-ion-driven resistive interchange mode in various NB injections in the LHD are studied using neutron emission profile measurements and numerical simulations using the orbit following model [13-15]. Although the fast ion transport and loss due to fast-ion-driven MHD instability in the LHD have been intensively studied, the information on the energy distribution of fast ions is necessary in order to understand the excitation of MHD instabilities. A powerful diagnostic to measure fast ion distribution is offered by the neutron emission spectrometer. Speaking about deuterium-deuterium neutron spectrometry, the compact neutron emission spectrometer based on the conventional liquid scintillation detector has been utilized in tokamaks using elastic collision of proton by fast-neutron [16, 17]. Unfolding is needed in this conventional technique because we only can observe the energy of recoil proton created by the elastic collision. Recently, a neutron emission spectrometer based on Cs_2LiYCl_6:Ce with 99% ^{7}Li-enrichment (the so-called CLYC7) scintillator has been developed. Unlike the liquid scintillator, the deuterium-deuterium fast neutrons are detected with the CLYC7 through the $^{35}Cl(n,p)^{35}S$ reactions. Because the CLYC7 scintillator utilizes energy of both reaction products, the unfolding technique is not fully required

except for energy resolution of the detector#18-20].#he tangential line-of-sight compact neutron emission spectrometer based on the CLYC7 detector (hereafter called the CNES) has been utilized to measure the neutron energy spectrum during N-NBs heated plasma since 2020 in the LHD. With the newly installed CNES fast ion distribution, reflecting on the neutron energy spectrum, can be measured. The first measurement of neutron energy spectrum using the CNES is presented in this paper.

2. Characteristic of CLYC7 scintillation detector

The CLYC7 scintillator with a diameter of 1 inch and a height of 1 inch [21], coupled with a conventional photomultiplier tube (PMT), (H10580-100-01, Hamamatsu Photonics K.K. [22]), is used in the CNES in the LHD. The detector is biased with a high voltage of -1.3 kV using a quad high voltage power supply (RPH-033, HAYASHI-REPIC Corp. [23]). The signal of the CLYC7 detector is fed into the data acquisition system (DAQ), equipped with a 12 bit/±2V analog-to-digital converter, with a sampling frequency of 250 MHz, with an online pulse shape discrimination function (DT5720B, CAEN [24]). The typical waveform of neutron and γ-ray induced pulse signals obtained by the CLYC7 detector is shown in Fig 1a). Here, the typical pulse width is approximately 1 μs. The charge integration method using pulse shape discrimination $\mathrm{PSD} = (Q_{\mathrm{total}} - Q_{\mathrm{fast}})/Q_{\mathrm{total}}$ is utilized for discriminating neutron and γ-ray pulses. Q_{total} is an integrated signal in t_{total} of 300 ns and Q_{fast} is an integrated signal in t_{fast} of 120 ns.

The CLYC7 detector is characterized using an accelerator-based neutron source in the Fast Neutron Laboratory (FNL) of the Tohoku University [25]. The Dynamitron accelerator with a maximum acceleration voltage of 3.0 MV and a maximum beam current of 3 μA is employed to create the fast neutron. The experiment was perfomed using same systems and cables as LHD experiment. We performed FNL experiments in room temperature as the LHD torus hall. In the experiment, the D(d,n)^{3}He reaction (Q-value of 3.27 MeV) was performed. The deuteron beam with an energy from 1.5 MeV to 3.0 MeV and with beam current of 0.5 μA was injected into deuterium gas target with thickness of 3 cm. Note that the beam line and deuterium gas target were separated using the Havar foil with thickness of 6.4 micron. The detector was placed at 115 degrees and 15 degrees from the beam axis. In this work, the spectrum of deuteron beam in the gas target were estimated via TRIM code [26]. Using simple two-body kinematic calculation and

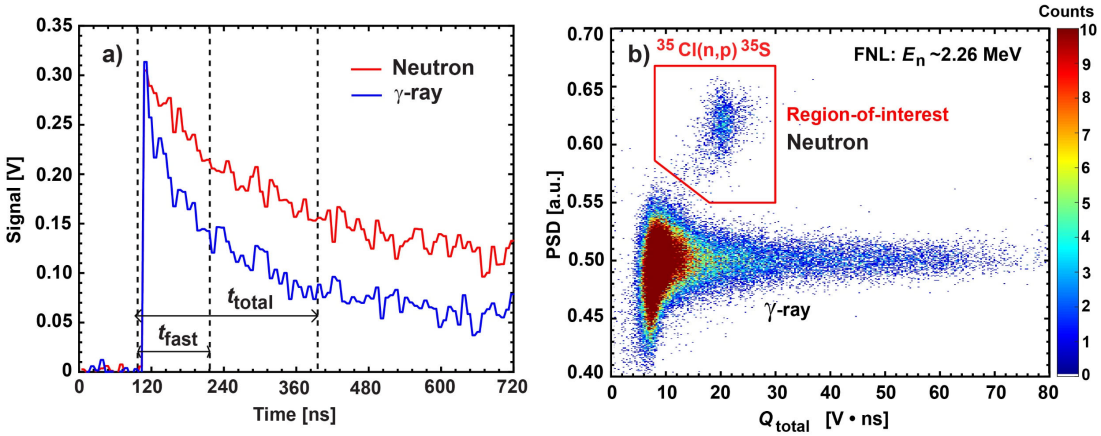

Figure 1. a) Typical signal of neutron and γ-ray induced in CLYC7 detector. b) Two-dimensional PSD plot of FNL experiment when E_n is ~2.26 MeV.

deuterium-deuterium nuclear cross-section of JENDL-4.0 [27], the neutron energy (E_n) at the detector position is calculated. The neutron energy at the detector in each experiment was calculated to be between approximately 2.26 MeV and 5.54 MeV. Figure 1b) shows an example of two-dimensional PSD plot when the E_n is ~2.26 MeV. The measured 2.26 MeV neutron is seen through the $^{35}Cl(n,p)^{35}S$ reaction channel showing in the region of interest. The resolution of the incident neutron energy of ~2.26 MeV is ~12%. The neutron energy resolution is larger than the expected of the equivalent γ-ray of 5%, as expected [20]. Using the calculated E_n of between 2.26 MeV and 5.54 MeV and the obtained Q_{total} corresponding to the $^{35}Cl(n,p)^{35}S$ reaction channel, the relation of Q_{total} [V•ns] = $10.94 \times E_{\mathrm{n}}[\mathrm{MeV}] + 1.51$ is obtained.

3. The compact neutron emission spectrometer in LHD

3.1 Experimental setup

The CNES is installed on the plasma midplane at the tangential LHD port (the so-called 6T port) with a tangency radius of ~3.65 m. Figure 2a) shows the top view of the LHD, three N-NBs, and the position of the CNES. N-NB#2 injects beam ions that move away from the CNES, whereas N-NB#1 and N-NB#3 inject beam ions that move toward the CNES. The injection energy of N-NBs is up to 180 keV. The tangency radius of N-NB#1, N-NB#2, and N-NB#3 are 3.75 m, 3.75 m, and 3.70 m, respectively.

The CNES is placed at a distance of ~1.4 m from the port flange. A cylindrical magnetic shield 1 cm thick, 7 cm in diameter, and 20 cm in length, made of SS400, was equipped to avoid the stray magnetic field effect on the PMT (see Fig. 2b) top). Since the CLYC7 detector has a sensitivity to γ-ray, the cylindrical γ-ray shielding made of lead 5 cm thick, 17 cm in diameter, and 30 cm in length, is installed. The outer layer is equipped with neutron shielding made of 10% doped borated polyethylene 30 cm in width, 60 cm in length, and 40 cm high, in order to suppress unwanted scattered neutrons. The insert collimator made of 10% doped borated polyethylene with a diameter of 3 cm is utilized in order to enhance directionality (see Fig. 2b) bottom). Figure 2c) shows an electronics schematic of the data acquisition system of the CNES.

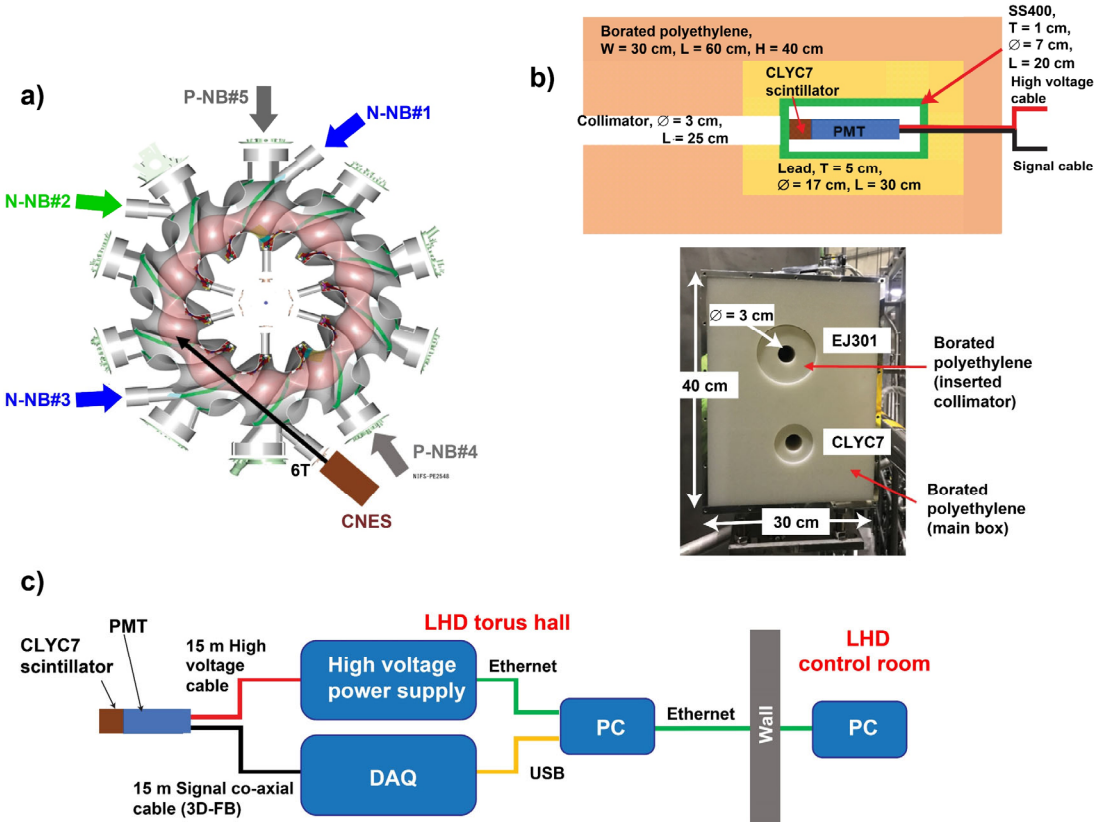

Figure 2. a) Schematic top view of LHD, N-NBs, and CNES. Black arrow indicates CNES sightline. b) Top: cut view of shielding box of CLYC7 detector; bottom: front view of shielding box. CLYC7 detector is placed inside lower hole providing viewing on plasma midplane. Note EJ301 detector beyond scope of this paper. c) Electronics schematic of CLYC7 detector in LHD.

3.2 Maximum counting rate capability

The operational capability of the CNES in the pulse counting rate is investigated in the LHD. Figure 3a) shows the time evolution of the total neutron emission rate (S_n), measured by the neutron flux monitor (NFM) [8, 28] , as well as the pulse counting rate of neutrons and γ-rays measured by the CNES, of plasma discharge #163510. The size of the time-bin for the CNES measurement is set at 40 ms. Note that the trigger time for the CNES is manually aligned to match the time trace of S_n, due to the lack of a data acquisition trigger. During the time between 3.3 s and 4.7 s, the pulse counting rate measured by the CNES increases consistently to the S_n. And then, the pulse counting rate suddenly drops at the time of approximately 4.7 s due to DAQ buffer overflows, when the pulse counting rate exceeds 1.2×10^3 counts per 40 ms, which corresponds to 30 kcps. Note that the dead time due to the pulse pileup is not significant ~3% at the 30 kcps. The capability of the CNES in the high S_n region was surveyed in the six deuterium plasma discharges. The pulse counting rate obtained by the CNES and S_n obtained by the NFM is compared (see Fig. 3b)). The result shows that the linearity of the pulse counting rate of the CNES is limited by approximately S_n of $\sim1.5\times10^{13}$ n/s.

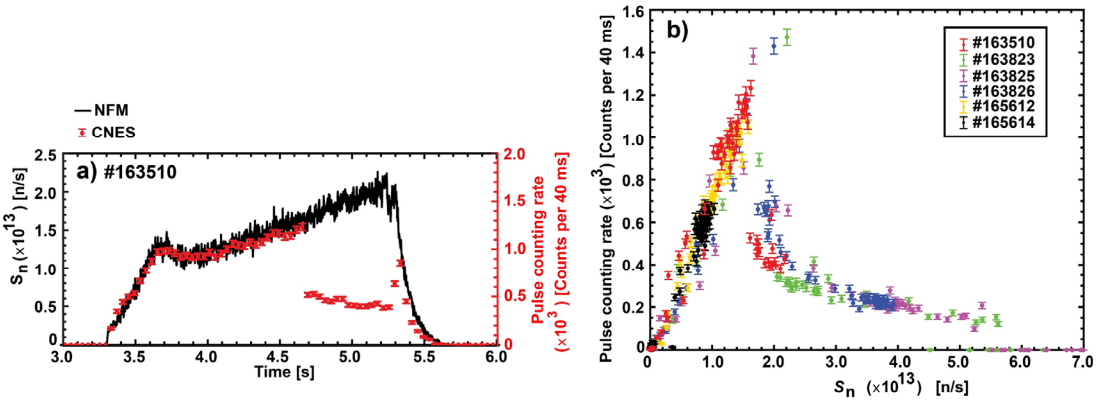

Figure 3. a) Time evolution of S_n measured by the NFM and pulse counting rate (neutron and γ-ray) measured by CNES of deuterium plasma discharge #163510. b) Comparison of pulse counting rate and S_n of six deuterium plasma discharges.

4. First neutron spectrum measurement using compact neutron emission spectrometer in LHD

Result of neutron energy spectrum during deuterium N-NBs heating in LHD deuterium plasma is reported here. The experiments were performed with the magnetic axis position in vacuum R_{ax_vac} of 3.9 m and a toroidal magnetic field strength B_T of 0.99 T with counter-clockwise (CCW) directions viewed from the top, to create relatively low-electron temperature plasmas for maintaining the low S_n. Figure 4 shows the waveform of plasma discharge #164277. In this discharge, line-averaged electron density n_{e_avg} is ~2×10^{18} m^{-3} and central electron temperature T_{e0} is ~0.6 keV. The time interval between 3.48 s and 4.26 s during simultaneous injection of N-NB#1 (injection energy E_{NB} = 179 keV), N-NB#2 (E_{NB} = 166 keV), and N-NB#3 (E_{NB} = 166 keV), is selected. In plasma discharge #164273, n_{e_avg} is ~5×10^{18} m^{-3}, T_{e0} is ~0.7 keV, and the selected time interval is between 4.82 s and 5.23 s when only N-NB#3 (E_{NB} = 166 keV) is injected. A two-

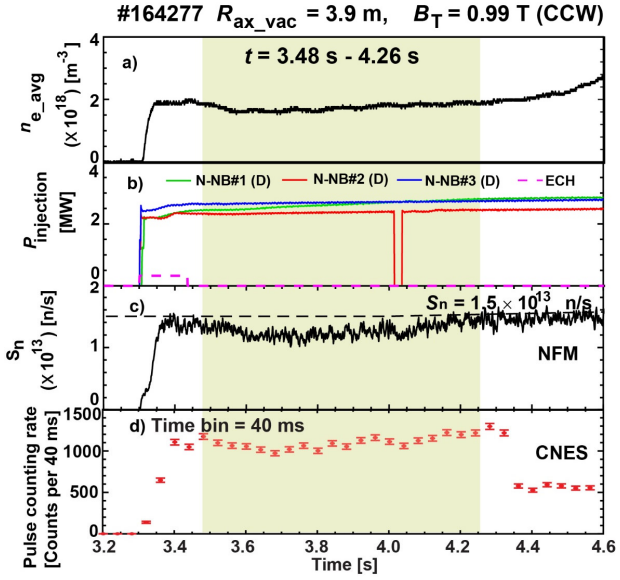

Figure 4. Time evolution of deuterium plasma discharge #164277. a) Line-averaged electron density n_{e_avg}, b) injected power of N-NB#1, N-NB#2, and N-NB#3, c) S_n measured by NFM, and d) pulse counting rate measured by CNES. Green-shaded areas indicate time interval selection to calculate neutron counts of CNES.

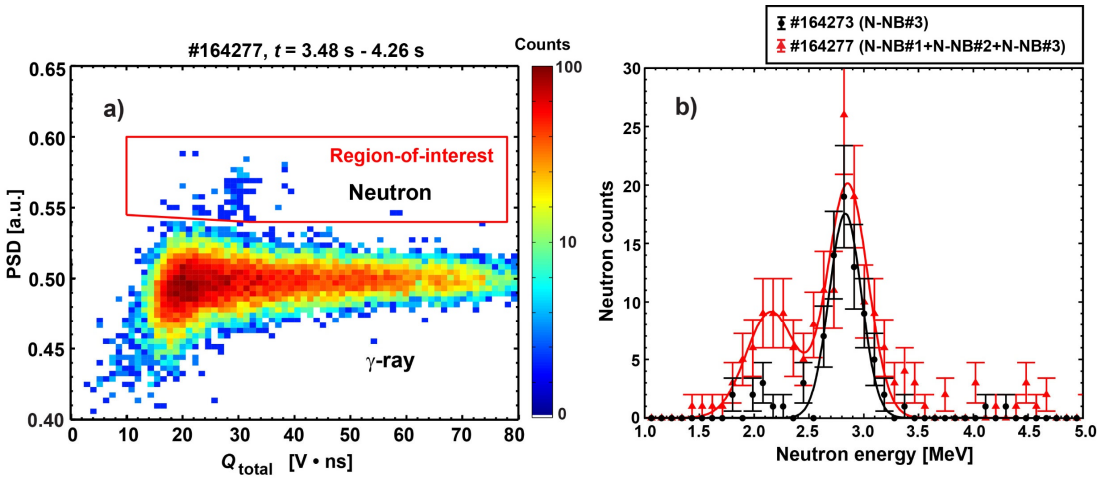

Figure 5. a) Two-dimensional PSD plot of deuterium plasma discharge #164277 during time interval between 3.48 s and 4.26 s. b) Neutron energy spectra during N-NBs heating of LHD deuterium plasma discharge #164273 and discharge #164277 measured by CNES.

dimensional PSD plot of plasma discharge #164277 during the selected time interval is presented in Fig. 5a). The neutrons measured through the $^{35}Cl(n,p)^{35}S$ reaction channel are seen in the region of interest. The neutron energy spectrum is shown in Fig. 5b). Two peaks at ~2.15 MeV and ~2.86 MeV are observed when N-NB#1, N-NB#2, and N-NB#3 are simultaneously injected, whereas only one peak at ~2.83 MeV is obtained when only N-NB#3 is injected. Upper shifted neutron energy corresponds to N-NB#1 and N-NB#3 ions moving toward the CNES. On the other hand, lower shifted neutron energy corresponds to N-NB#2 ions moving away from the CNES.

Further, the neutron energies observed by the CNES are compared to the virgin deuterium-deuterium neutron energies expected by the simple two-body kinematic calculation. In the calculation, we assumed that the cold deuteron and deuteron beam with an energy of 179 keV for N-NB#1 and 166 keV for N-NB#2 and N-NB#3 are fused at the magnetic axis position. Angles of the CNES line-of-sight to the N-NB#1, N-NB#2, and N-NB#3 injection axis are approximately 42 degrees, 140 degrees, and 45 degrees, respectively. Considering the viewing angle of the CNES and the N-NB injection angles, the virgin deuterium-deuterium neutron energies observed by the CNES are calculated to be approximately 2.87 MeV, 2.17 MeV, and 2.84 MeV for N-NB#1, N-NB#2, and N-NB#3 ions, respectively. The difference of upper shifted neutron energy of approximately 30 keV shown in Fig. 5b) is mainly due to the difference of N-NB#1 and N-NB#3 injection angles and injection energies. It is found that the experimentally obtained Doppler shift in neutron energies are almost consistent with those expected from simple two-body kinematics.

5. Summary

The CNES based on the CLYC7 scintillator is newly installed in the LHD in order to measure neutron energy spectra, reflecting the fast ion energy distribution in N-NBs heated plasmas. The first neutron spectroscopy using the CNES is performed in an LHD deuterium plasma experiment. The Doppler shift in neutron energy according to the N-NB injection direction is successfully measured. The upper shifted neutron energy and lower shifted neutron energy are observed when the fast ions move toward and move away from the CNES, respectively. The peaks of neutron energy observed by the CNES are almost consistent with the neutron energies expected

from the simple two-body kinematic calculation. Further, the detailed comparison of the neutron energy obtained in experiments and calculations using a drift kinetic code, e.g., GNET [29], will be conducted in our future work.

Acknowledgments

This research was partly supported by NIFS Collaboration Research programs (KOAH037), by the NINS program of Promoting Research by Networking among Institutions (Grant Number 01411702), the Japan-China Post-Core-University-Program called Post-CUP, and by the Excellence Program of Hefei Science Center CAS (No.2020HSC-UE012). We are pleased to acknowledge the assistance of the LHD Experiment Group.

References

[1] A. Fasoli *et al*., Nucl. Fusion **47**, S264 (2007).
[2] W. W. Heidbrink, Phys. Plasma **15**, 055501 (2008).
[3] K. Toi *et al*., Plasma Phys. Control. Fusion **53**, 024008 (2011).
[4] M. Osakabe *et al*., Nucl. Fusion **46**, S911 (2006).
[5] K. Ogawa *et al*., Nucl. Fusion **50**, 084005 (2010).
[6] K. Ogawa *et al*., Nucl. Fusion **52**, 094013 (2012).
[7] R. Seki *et al*., Nucl. Fusion **59**, 096018 (2019).
[8] M. Isobe *et al*., IEEE Trans. Plasma Sci. **46**, 2050 (2018).
[9] M. Isobe *et al*., Nucl. Fusion **58**, 082004 (2018).
[10] K. Ogawa *et al*., Nucl. Fusion **59**, 076017 (2019).
[11] K. Ogawa *et al*., Plasma Fusion Res. **16**, 1102023 (2021).
[12] M. Osakabe et al., Fusion Sci. Technol. **72,** 199 (2017).
[13] K. Ogawa *et al*., Plasma Phys. Control. Fusion **60**, 044005 (2018).
[14] K. Ogawa *et al*., Nucl. Fusion **60**, 112011 (2020).
[15] K. Ogawa et al., Nuclear Fusion **61**, 096035 (2021).
[16] G. Tardini et al., Rev. Sci. Instrum. **87**, 103504 (2016).
[17] Y. M. Zhang et al., Rev. Sci. Instrum. **89**, 10I141 (2018).
[18] D. Rigamonti *et al*., J. Instrum **14**, C09025 (2019).
[19] N. D'Olympia *et al*., Nucl. Instrum. Methods Phys. A **763**, 433-441 (2014).
[20] A. Giaz *et al*., Nucl. Instrum. Methods Phys. A **825**, 51-61 (2016).
[21] See https://www.dynasil.com/product-category/scintillators/clyc-gamma-neutron-scintillators/ for the specification of the CLYC7 scintillator.
[22] See https://www.hamamatsu.com/resources/pdf/etd/High_energy_PMT_TPMZ0003E.pdf for PMT H10580-100-01, Hamamatsu Photonics K.K.
[23] See https://www.h-repic.co.jp/pdf/RPH-034.pdf for Quad high voltage power supply.
[24] See https://www.caen.it/products/dt5720/ for CAEN, UM 3244, DT5720B.
[25] M. Baba *et al*., Nucl. Instrum. Methods Phys. A **376**, 115-123 (1996).
[26] See http://www.srim.org/ for TRIM code.
[27] JENDL 4.0 nuclear reaction cross-section.
[28] D. Ito et al., Plasma Fusion Res. **16** 1405018 (2021).
[29] H. Yamaguchi and S. Murakami, Nucl. Fusion **56**, 026003 (2016).